A semi-implicit FEM-FCT algorithm for efficient treatment of time-dependent problems

D. Kuzmin[1]

Institute of Applied Mathematics (LS III), University of Dortmund
Vogelpothsweg 87, D-44227, Dortmund, Germany

D. Kourounis

Department of Material Sciences and Engineering
University of Ioannina, Greece

Abstract

A new generalization of the flux-corrected transport (FCT) methodology to implicit finite element discretizations is proposed. The underlying high-order scheme is supposed to be unconditionally stable and produce time-accurate solutions to evolutionary convection problems. Its nonoscillatory low-order counterpart is constructed by means of mass lumping followed by elimination of negative off-diagonal entries from the discrete transport operator. The raw antidiffusive fluxes, which represent the difference between the high- and low-order schemes, are updated and limited within an outer defect correction loop. The upper bound for the magnitude of each antidiffusive flux is evaluated using a single sweep of the multidimensional FCT limiter at the first outer iteration. This semi-implicit limiting strategy makes it possible to enforce the positivity constraint in a very robust and efficient manner. Moreover, the computation of an intermediate low-order solution can be avoided. Numerical examples are presented for two-dimensional benchmark problems discretized by the standard Galerkin FEM combined with the Crank-Nicolson time-stepping.

Key Words: high-resolution schemes; flux-corrected transport algorithm; finite element method; implicit time discretization

1 Introduction

The advent of nonlinear high-resolution schemes for convection-dominated flows traces its origins to the *flux-corrected transport* (FCT) methodology introduced in the early 1970s by Boris and Book [1]. The fully multidimensional generalization proposed by Zalesak [23] has formed a very general framework for the design of FCT algorithms by representing them as a blend of linear high- and low-order approximations. Unlike other limiting techniques, which are typically based on geometric design criteria, flux correction of FCT

[1]Correspondence to: kuzmin@math.uni-dortmund.de

type is readily applicable to finite element discretizations on unstructured meshes [16],[18]. A comprehensive summary of the state of the art can be found in [2],[12],[18],[25].

The design philosophy behind modern front-capturing methods involves a set of physical or mathematical constraints to be imposed on the discrete solution so as to prevent the formation of spurious undershoots and overshoots in the vicinity of steep gradients. To this end, the following algorithmic components are to be specified [12],[25]

- a high-order approximation which may fail to possess the desired properties;
- a low-order approximation which does enjoy these properties but is less accurate;
- a way to decompose the difference between the above into a sum of skew-symmetric internodal fluxes which can be manipulated without violating mass conservation;
- a cost-effective mechanism for adjusting these antidiffusive fluxes in an adaptive fashion so that the imposed constraints are satisfied for a given solution.

Classical FCT algorithms are based on an explicit correction of the low-order solution whose local extrema serve as the upper/lower bounds for the sum of limited antidiffusive fluxes. In the case of an implicit time discretization, which gives rise to a nonlinear algebraic system, the same strategy can be used to secure the positivity of the right-hand side, whereas the left-hand side is required to satisfy the *M-matrix* property [7],[8].

The rationale for the development of implicit FCT algorithms stems from the fact that the underlying linear discretizations must be stable. In particular, the use of an unstable high-order method may give rise to nonlinear instabilities which manifest themselves in significant distortions of the solution profiles as an aftermath of aggressive flux limiting. In the finite element context, a proper amount of streamline diffusion can be used to stabilize an explicit high-order scheme based on the standard Galerkin approximation. However, the evaluation of extra terms increases the cost of matrix assembly and the time step must satisfy a restrictive 'CFL' condition. On the other hand, unconditionally stable implicit methods can be operated at large time steps (unless iterative solvers fail to converge or the positivity criterion is violated) and there is no need for any extra stabilization. Moreover, the overhead cost is insignificant, since the use of a consistent mass matrix leads to a sequence of linear systems even in the fully explicit case.

The generalized FEM-FCT methodology introduced in [7],[8] and refined in [9],[10] is applicable to implicit time discretizations but the cost of iterative flux correction is rather high if the sum of limited antidiffusive fluxes and the nodal correction factors need to be updated in each outer iteration. In addition, the nonlinear convergence rates leave a lot to be desired in many cases. The use of 'frozen' correction factors computed at the beginning of the time step by the standard Zalesak limiter alleviates the convergence problems but the linearized scheme can no longer be guaranteed to remain positivity-preserving. The semi-implicit limiting strategy proposed in the present paper makes it possible to overcome this problem and enforce the positivity constraint at a cost comparable to that of explicit flux correction. The resulting FEM-FCT algorithm is to be recommended for strongly time-dependent problems discretized in time by the second-order accurate Crank-Nicolson scheme. The design of general-purpose flux limiters which are more expensive but do not suffer from a loss of accuracy at large time steps is addressed in [14].

2 Algebraic flux correction

In this paper, we adopt an algebraic approach to the design of high-resolution schemes which consists of imposing certain mathematical constraints on discrete operators, so as to achieve some favorable matrix properties. A very handy algebraic criterion, which represents a multidimensional generalization of Harten's TVD theorem, was introduced by Jameson [4],[5] who proved that a semi-discrete scheme of the form

$$\frac{\mathrm{d}u_i}{\mathrm{d}t} = \sum_{j\neq i} c_{ij}(u_j - u_i), \qquad c_{ij} \geq 0, \quad \forall j \neq i \tag{1}$$

is *local extremum diminishing* (LED). After the discretization in time, such schemes remain positivity-preserving (PP) provided that each solution update $u^n \;\rightarrow\; u^{n+1}$ or the converged steady-state solution $u^{n+1} = u^n$ satisfy an algebraic system of the form

$$Au^{n+1} = Bu^n, \tag{2}$$

where $A = \{a_{ij}\}$ is an *M-matrix* and $B = \{b_{ij}\}$ has no negative entries. Under these conditions, the positivity of the old solution carries over to the new one [10],[12]

$$u^n \geq 0 \qquad \Rightarrow \qquad u^{n+1} = A^{-1}Bu^n \geq 0. \tag{3}$$

If the underlying spatial discretization is LED, then the off-diagonal coefficients of both matrices have the right sign, while the positivity condition $b_{ii} \geq 0$ for the diagonal entries of B yields a readily computable upper bound for admissible time steps [12]

$$1 + \Delta t(1-\theta)\min_i c_{ii}^n \geq 0 \qquad \text{for} \quad 0 \leq \theta < 1. \tag{4}$$

Of course, the above algebraic constraints are not the necessary but merely sufficient conditions for a numerical scheme to be local extremum diminishing and/or positivity preserving. In the linear case, they turn out to be far too restrictive. According to the well-known Godunov theorem, linear schemes satisfying these criteria are doomed to be (at most) first-order accurate. On the other hand, a high-order discretization which fails to satisfy the imposed constraints unconditionally can be adjusted so that it admits an equivalent representation of the form (1) and/or (2), where the matrix entries may depend on the unknown solution. This idea makes it possible to construct a variety of nonlinear high-resolution schemes based on the *algebraic flux correction* paradigm [12],[14].

To keep the presentation self-contained, we will follow the roadmap displayed in Fig. 1 and explain the meaning of all discrete operators in the next three sections. Roughly speaking, a high-order Galerkin discretization is to be represented in the form

$$Au^{n+1} = Bu^n + f, \tag{5}$$

where the matrices A and B satisfy the positivity constraint (2). In order to guarantee that the extra term f poses no hazard to positivity, it is replaced by its limited counterpart f^* such that the right-hand side remains nonnegative for $u^n \geq 0$. This modification is mass-conserving provided that both f and f^* can be decomposed into skew-symmetric

1. Semi-discrete high-order scheme (Galerkin FEM)

$$M_C \frac{\mathrm{d}u}{\mathrm{d}t} = Ku \qquad \text{such that} \quad \exists\, j \neq i:\ k_{ij} < 0$$

2. Semi-discrete low-order scheme $L = K + D$

$$M_L \frac{\mathrm{d}u}{\mathrm{d}t} = Lu \qquad \text{such that} \quad l_{ij} \geq 0,\ \forall j \neq i$$

3. Nonlinear FEM-FCT algorithm $Au^{n+1} = Bu^n + f^*$,

where $A = M_L - \theta \Delta t L, \quad B = M_L + (1-\theta)\Delta t L$

Figure 1: Roadmap of matrix manipulations.

internodal fluxes as defined below. A family of implicit FEM-FCT schemes based on this algebraic approach was proposed in [7],[8] and combined with an iterative limiting strategy in [10]. In Section 5.2, we present an alternative generalization of Zalesak's limiter which proves much more robust and efficient. The new approach to flux correction of FCT type is also based on the positivity constraint (2) but enforces it in another way so that the costly computation of nodal correction factors is performed just once per time step. The positivity of the resulting semi-implicit FCT algorithm will be proven in Section 5.3.

3 Semi-discrete high-order scheme

As a standard model problem, consider the time-dependent continuity equation for a scalar quantity u transported by the velocity field $\mathbf{v}$ which is assumed to be known

$$\frac{\partial u}{\partial t} + \nabla \cdot (\mathbf{v}u) = 0. \tag{6}$$

Let the discretization in space be performed by a (Galerkin) finite element method which yields a DAE system for the vector of time-dependent nodal values

$$M_C \frac{\mathrm{d}u}{\mathrm{d}t} = Ku, \tag{7}$$

where $M_C = \{m_{ij}\}$ denotes the consistent mass matrix and $K = \{k_{ij}\}$ is the discrete transport operator. The latter may contain some streamline diffusion used for stabilization purposes and/or to achieve better phase accuracy in the framework of Taylor-Galerkin methods [3]. Its skew-symmetric part $\frac{1}{2}(K - K^T)$ is consistent with the properties of the continuous convective derivative $\mathbf{v} \cdot \nabla$ and implies the conservation of kinetic energy in turbulent flow computations, see [21],[22]. At the same time, the symmetric part given by $\frac{1}{2}(K + K^T) - \mathrm{diag}\{K\}$ represents a discrete (anti-)diffusion operator, which results in a nonphysical but sometimes desirable production or dissipation of kinetic energy.

4 Semi-discrete low-order scheme

In the linear case, the algebraic constraints (1) and (2) can be readily enforced by means of 'discrete upwinding' as proposed in [7],[8]. For a semi-discrete finite element scheme of the form (7), the required matrix manipulations are as follows

- replace the consistent mass matrix M_C by its lumped counterpart $M_L = \mathrm{diag}\{m_i\}$,
- render the operator K local extremum diminishing by adding an artificial diffusion operator $D = \{d_{ij}\}$ so as to eliminate all negative off-diagonal coefficients.

This straightforward 'postprocessing' transforms (7) into its linear LED counterpart

$$M_L \frac{\mathrm{d}u}{\mathrm{d}t} = Lu, \qquad L = K + D, \tag{8}$$

where D is supposed to be a symmetric matrix with zero row and column sums. For each pair of nonzero off-diagonal coefficients k_{ij} and k_{ji} of the high-order operator K, the optimal choice of the artificial diffusion coefficient d_{ij} reads [8],[12]

$$d_{ij} = \max\{-k_{ij}, 0, -k_{ji}\} = d_{ji}. \tag{9}$$

Alternatively, one can apply discrete upwinding to the skew-symmetric part $\frac{1}{2}(K - K^T)$ of the original transport operator K, which corresponds to [14]

$$d_{ij} = \frac{|k_{ij} - k_{ji}|}{2} - \frac{k_{ij} + k_{ji}}{2} = d_{ji}. \tag{10}$$

In either case, the off-diagonal coefficients of the low-order operator $l_{ij} := k_{ij} + d_{ij}$ are nonnegative, as required by the LED criterion (1). Due to the zero row sum property of the artificial diffusion operator D, the diagonal coefficients of L are given by

$$l_{ii} := k_{ii} - \sum_{j \neq i} d_{ij}. \tag{11}$$

The semi-discretized equation for the nodal value $u_i(t)$ can be represented as

$$m_i \frac{\mathrm{d}u_i}{\mathrm{d}t} = \sum_{j \neq i} l_{ij}(u_j - u_i) + u_i \sum_j k_{ij}, \tag{12}$$

where $m_i = \sum_j m_{ij} > 0$ and $l_{ij} \geq 0$, $\forall i \neq j$. The last term in the above expression represents a discrete counterpart of $-u\nabla \cdot \mathbf{v}$ which is responsible for a physical growth of local extrema [12]. In the semi-discrete case, it is harmless since (cf. [6])

$$u_i(t) = 0, \quad u_j(t) \geq 0, \quad \forall j \neq i \qquad \Rightarrow \qquad \frac{\mathrm{d}u_i}{\mathrm{d}t} \geq 0, \tag{13}$$

which proves that the low-order scheme (8) is positivity-preserving. For the fully discrete system to inherit this property, the time step should be chosen in accordance with the CFL-like condition (4) unless the backward Euler time-stepping ($\theta = 1$) is employed.

5 Nonlinear FEM-FCT algorithm

The high-order system (7) discretized in time by a standard two-level θ-scheme

$$[M_C - \theta\Delta tK]u^{n+1} = [M_C + (1-\theta)\Delta tK]u^n \tag{14}$$

admits an equivalent representation in the form (5) amenable to flux correction

$$[M_L - \theta\Delta tL]u^{n+1} = [M_L + (1-\theta)\Delta tL]u^n + f(u^{n+1}, u^n). \tag{15}$$

The last term in the right-hand side is assembled from skew-symmetric internodal fluxes f_{ij} which can be associated with the edges of the sparsity graph [12]

$$f_i = \sum_{j\neq i} f_{ij}, \qquad \text{where} \quad f_{ji} = -f_{ij}. \tag{16}$$

Specifically, these *raw antidiffusive fluxes*, which offset the discretization error induced by mass lumping and discrete upwinding, are given by the formula [10],[12]

$$f_{ij} = [m_{ij} + \theta\Delta td_{ij}^{n+1}]\ (u_i^{n+1} - u_j^{n+1}) - [m_{ij} - (1-\theta)\Delta td_{ij}^n]\ (u_i^n - u_j^n). \tag{17}$$

Interestingly enough, the contribution of the consistent mass matrix consists of a truly antidiffusive implicit part and a diffusive explicit part which has a strong damping effect. In fact, explicit mass diffusion of the form $(M_C - M_L)u^n$ has been used to construct the 'monotone' low-order method in the framework of explicit FEM-FCT algorithms [16].

In the case of an implicit time discretization ($0 < \theta \leq 1$), the nonlinearities inherent to the governing equation and/or to the employed high-resolution scheme call for the use of an iterative solution strategy. Let successive approximations to the solution u^{n+1} be computed step-by-step in the framework of a fixed-point defect correction scheme [12]. Each solution update amounts to solving a linear system of the form (15) which reads

$$Au^{(m+1)} = b^{(m)}, \qquad m = 0, 1, 2\ldots. \tag{18}$$

This fixed point iteration is preconditioned by the 'monotone' low-order operator

$$A = M_L - \theta\Delta tL \tag{19}$$

which enjoys the M-matrix property, since the off-diagonal entries of L are nonnegative by construction. The right-hand side $b^{(m)}$, which needs to be updated in each outer iteration, consists of a low-order part augmented by limited antidiffusion [12]

$$b^{(m)} = Bu^n + f^*(u^{(m)}, u^n), \qquad B = M_L + (1-\theta)\Delta tL. \tag{20}$$

In order to prevent the formation of nonphysical undershoots and overshoots, the raw antidiffusive fluxes f_{ij} should be multiplied by suitable correction factors so that

$$f_i^* = \sum_{j\neq i} \alpha_{ij} f_{ij}, \qquad \text{where} \qquad 0 \leq \alpha_{ij} \leq 1. \tag{21}$$

This adjustment transforms (15) into a nonlinear combination of the low-order scheme ($\alpha_{ij} \equiv 0$) and the original high-order one ($\alpha_{ij} \equiv 1$). The task of the flux limiter is to determine an optimal value of each correction factor α_{ij} individually so as to remove as much artificial diffusion as possible without violating the positivity constraint.

5.1 Semi-explicit FCT limiter

The first implicit FCT algorithm for finite element discretizations on unstructured meshes [7],[8] was based on the following limiting strategy which was eventually superseded by further extensions proposed in a series of subsequent publications [9],[10]

1. Compute the high-order solution to (15) in an iterative way by solving (18) using the total amount of raw antidiffusion ($\alpha_{ij} \equiv 1$) to assemble the term f^*.

2. Evaluate the contribution of the consistent mass matrix to the raw antidiffusive fluxes (17) using the converged high-order solution as a substitute for u^{n+1}.

3. Solve the explicit subproblem $M_L\tilde{u} = Bu^n$ for the positivity-preserving intermediate solution $\tilde{u}$ which represents an explicit low-order approximation to $u(t^{n+1-\theta})$.

4. Invoke Zalesak's multidimensional FCT limiter to determine the correction factors α_{ij} so as to secure the positivity of the right-hand side as explained below.

5. Compute the final solution by solving the linear system $Au^{n+1} = b$, where

$$b_i = m_i\tilde{u}_i + \sum_{j\neq i} f_{ij}^*, \qquad f_{ij}^* = \alpha_{ij} f_{ij}. \tag{22}$$

In the fully explicit case, we have $A = M_L$ so that $u^{n+1} = M_L^{-1}b$ can be computed explicitly, and the classical FEM-FCT algorithm of Löhner *et al.* [16],[18] is recovered. The crux of the above generalization lies in the special choice of the preconditioner A which guarantees that the positivity of the right-hand side is preserved, whence

$$\tilde{u} \geq 0 \quad \Rightarrow \quad b \geq 0 \quad \Rightarrow \quad u^{n+1} = A^{-1}b \geq 0. \tag{23}$$

The flux correction process starts with an optional 'prelimiting' of the raw antidiffusive fluxes f_{ij}. It consists of cancelling the 'wrong' ones which tend to flatten the intermediate solution and create numerical artifacts. The required adjustment is given by [14]

$$f_{ij} := \max\{0, p_{ij}\}(\tilde{u}_i - \tilde{u}_j), \qquad p_{ij} = f_{ij}/(\tilde{u}_i - \tilde{u}_j). \tag{24}$$

The remaining fluxes are truly antidiffusive and need to be limited. The upper and lower bounds to be imposed on the net antidiffusive flux depend on the local extrema

$$\tilde{u}_i^{\max} = \max_{j\in S_i} \tilde{u}_j, \qquad \tilde{u}_i^{\min} = \min_{j\in S_i} \tilde{u}_j, \tag{25}$$

where $S_i = \{j \,|\, m_{ij} \neq 0\}$ denotes the set of nodes which share an element/edge with node i so that the basis functions φ_i and φ_j have overlapping supports.

In the worst case, all antidiffusive fluxes into node i have the same sign. Hence, it is worthwhile to treat the positive and negative ones separately, as proposed by Zalesak [23]

1. Evaluate the sums of all positive and negative antidiffusive fluxes into node i

$$P_i^+ = \sum_{j\neq i} \max\{0, f_{ij}\}, \qquad P_i^- = \sum_{j\neq i} \min\{0, f_{ij}\}. \tag{26}$$

2. Compute the distance to a local maximum/minimum of the low-order solution

$$Q_i^+ = \tilde{u}_i^{\max} - \tilde{u}_i, \qquad Q_i^- = \tilde{u}_i^{\min} - \tilde{u}_i. \tag{27}$$

3. Calculate the nodal correction factors which prevent overshoots/undershoots

$$R_i^+ = \min\{1, m_i Q_i^+ / P_i^+\}, \qquad R_i^- = \min\{1, m_i Q_i^- / P_i^-\}. \tag{28}$$

4. Check the sign of f_{ij} and apply $R_i^\pm$ or $R_j^\mp$, whichever is smaller, so that

$$\alpha_{ij} = \begin{cases} \min\{R_i^+, R_j^-\}, & \text{if } f_{ij} > 0, \\ \min\{R_i^-, R_j^+\}, & \text{otherwise.} \end{cases} \tag{29}$$

This symmetric limiting strategy guarantees that the corrected right-hand side (22) satisfies the constraint $\tilde{u}_i^{\min} \le b_i/m_i \le \tilde{u}_i^{\max}$. Due to the fact that the preconditioner A was designed to be an M-matrix, the resulting scheme proves positivity-preserving [8],[12].

It is worth mentioning that the constituents of the sums $P_i^\pm$ vary with Δt, while the corresponding upper/lower bounds $Q_i^\pm$ are fixed. Consequently, the correction factors α_{ij} produced by Zalesak's limiter depend on the time step. This dependence, which is typical of FCT methods, turns out to be a blessing and a curse at the same time. On the one hand, a larger portion of the raw antidiffusive flux f_{ij} may be retained as the time step is refined. On the other hand, the accuracy of FCT algorithms deteriorates as Δt increases, since the positivity constraint (2) becomes too restrictive. The iterative limiting strategy proposed in [10] alleviates this problem to some extent by adjusting the correction factors α_{ij} in each outer iteration so as to recycle the rejected antidiffusion step-by-step. However, the cost of iterative flux correction is rather high and severe convergence problems may occur. Therefore, other limiting techniques such as the general-purpose (GP) flux limiter introduced in [14] are to be preferred for marching the solution to a steady state.

5.2 Semi-implicit FCT limiter

For truly time-dependent problems, the use of moderately small time steps is dictated by accuracy considerations so that flux limiting of FCT type is appropriate. In this case, the underlying time-stepping method should provide (unconditional) stability and be at least second-order accurate in order to capture the evolutionary details. For this reason, we favor an implicit time discretization of Crank-Nicolson type ($\theta = 1/2$) and mention the strongly A-stable fractional-step $\theta-$scheme [19] as a promising alternative.

The semi-explicit limiting strategy presented in the previous section can be classified as an algorithm of predictor-corrector type since the implicit part of the raw antidiffusive flux (17) is evaluated using the converged high-order solution in place of u^{n+1}. This handy linearization, which can be traced back to the classical FEM-FCT procedure [16], makes it possible to perform flux correction in a very efficient way, since Zalesak's limiter is invoked just once per time step. However, a lot of CPU time needs to be invested in the iterative solution of the ill-conditioned high-order system and the convergence may even fail if the time step is too large. Moreover, the final solution fails to satisfy the nonlinear

algebraic system (18) upon substitution. On the other hand, the update of $P_i^{\pm}$, $Q_i^{\pm}$, and $R_i^{\pm}$ in each outer iteration would trigger the cost of flux limiting and compromise the benefits of implicit time-stepping. In order to circumvent this problem, let us introduce an efficient semi-implicit FCT algorithm which can be implemented as follows:

- At the first outer iteration ($m = 1$), compute a set of antidiffusive fluxes $\tilde{f}_{ij}$ which provide an explicit estimate for the admissible magnitude of $f_{ij}^* = \alpha_{ij} f_{ij}$

  1. Initialize all auxiliary arrays by zeros: $P_i^{\pm} \equiv 0,\ Q_i^{\pm} \equiv 0,\ R_i^{\pm} \equiv 0.$

  2. Compute the positivity-preserving intermediate solution of low order

$$\tilde{u} = u^n + (1-\theta)\Delta t M_L^{-1} L u^n. \tag{30}$$

  3. For each pair of neighboring nodes i and j, evaluate the raw antidiffusive flux

$$f_{ij}^n = \Delta t d_{ij}^n (u_i^n - u_j^n) \tag{31}$$

  and add its contribution to the sums of positive/negative edge contributions

$$P_i^{\pm} := P_i^{\pm} + \begin{matrix}\max\\ \min\end{matrix}\{0, f_{ij}^n\}, \qquad P_j^{\pm} := P_j^{\pm} + \begin{matrix}\max\\ \min\end{matrix}\{0, -f_{ij}^n\}. \tag{32}$$

  4. Update the maximum/minimum admissible increments for both nodes

$$Q_i^{\pm} := \begin{matrix}\max\\ \min\end{matrix}\left\{Q_i^{\pm}, \tilde{u}_j - \tilde{u}_i\right\}, \qquad Q_j^{\pm} := \begin{matrix}\max\\ \min\end{matrix}\left\{Q_j^{\pm}, \tilde{u}_i - \tilde{u}_j\right\}. \tag{33}$$

  5. Relax the constraint $R_i^{\pm} \le 1$ for the nodal correction factors and compute

$$R_i^{\pm} := m_i Q_i^{\pm} / P_i^{\pm}. \tag{34}$$

  6. Multiply the raw antidiffusive fluxes f_{ij}^n by the minimum of $R_i^{\pm}$ and $R_j^{\mp}$

$$\tilde{f}_{ij} = \begin{cases} \min\{R_i^+, R_j^-\} f_{ij}^n, & \text{if } f_{ij}^n > 0, \\ \min\{R_i^-, R_j^+\} f_{ij}^n, & \text{otherwise.} \end{cases} \tag{35}$$

- At each outer iteration ($m = 1, 2, \ldots$), assemble f^* and plug it into (20)

  1. Update the target flux (17) using the solution from the previous iteration

$$\begin{aligned} f_{ij} &= [m_{ij} + \theta \Delta t d_{ij}^{(m)}](u_i^{(m)} - u_j^{(m)}) \\ &- [m_{ij} - (1-\theta)\Delta t d_{ij}^n]\ (u_i^n - u_j^n). \end{aligned} \tag{36}$$

  2. Constrain each flux f_{ij} so that its magnitude is bounded by that of $\tilde{f}_{ij}$

$$f_{ij}^* = \begin{cases} \min\{f_{ij}, \max\{0, \tilde{f}_{ij}\}\}, & \text{if } f_{ij} > 0, \\ \max\{f_{ij}, \min\{0, \tilde{f}_{ij}\}\}, & \text{otherwise.} \end{cases} \tag{37}$$

3. Insert the limited antidiffusive fluxes f_{ij}^* into the right-hand side (20)

$$b_i^{(m)} := b_i^{(m)} + f_{ij}^*, \qquad b_j^{(m)} := b_j^{(m)} - f_{ij}^*. \tag{38}$$

Due to the fact that f_{ij}^n is not the real target flux but merely an explicit predictor used to estimate the maximum amount of admissible antidiffusion, the multipliers $R_i^{\pm}$ are redefined so that the ratio $\tilde{f}_{ij}/f_{ij}^n$ may exceed unity. However, the effective correction factors $\alpha_{ij} := f_{ij}^*/f_{ij}$ are bounded by 0 and 1, as required for consistency.

Instead of computing the optimal upper/lower bounds (27) for a given time step, it is also possible to use some reasonable fixed bounds and adjust the time step if this is necessary to satisfy a CFL-like condition (as in the case of TVD methods). For instance, the auxiliary quantities $Q_i^{\pm}$ can be computed using u^n instead of $\tilde{u}$

$$Q_i^+ = \max_{j\in S_i} u_j^n - u_i^n, \qquad Q_i^- = \min_{j\in S_i} u_j^n - u_i^n. \tag{39}$$

The corresponding nodal correction factors $R_i^{\pm}$ should be redefined as [14]

$$R_i^{\pm} = (m_i - m_{ii})Q_i^{\pm}/P_i^{\pm}, \tag{40}$$

where $m_i - m_{ii} = \sum_{j\neq i} m_{ij}$ is the difference between the diagonal entries of the consistent and lumped mass matrices. This modification eliminates the need for evaluation of the intermediate solution $\tilde{u}$ in (30) and leads to a single-step FCT algorithm.

For a given time step, the multipliers (40) will typically be smaller than those defined by (34). However, in either case the denominator $P_i^{\pm}$ is proportional to Δt. Therefore, the difference between the effective correction factors α_{ij} will shrink and eventually vanish as the time step is refined. As long as Δt is sufficiently small, the accuracy of both FCT techniques depends solely on the choice of the underlying high-order scheme.

5.3 Positivity proof

The positivity proof for the semi-implicit FCT algorithm (30)–(38) follows that for the classical Zalesak limiter, see [8],[12]. In the nontrivial case $f_i^* \neq 0$, the $i-$th component of the right-hand side (20) admits the following representation

$$b_i^* = m_i\tilde{u}_i + f_i^* = (m_i - \alpha_i)\tilde{u}_i + \alpha_i\tilde{u}_k, \tag{41}$$

where the coefficient $\alpha_i = f_i^*/(\tilde{u}_k - \tilde{u}_i)$ is defined in terms of the local extremum

$$\tilde{u}_k = \begin{cases} \tilde{u}_i^{\max}, & \text{if } f_i^* > 0, \\ \tilde{u}_i^{\min}, & \text{if } f_i^* < 0. \end{cases} \tag{42}$$

This definition implies that $f_i^* = \alpha_i Q_i^{\pm}$, where $\alpha_i > 0$. By virtue of (41), the sign of the intermediate solution $\tilde{u}$ is preserved if the inequality $m_i - \alpha_i \geq 0$ holds.

In the case $f_i^* < 0$, the antidiffusive correction to node i is bounded from below by

$$m_i Q_i^- \leq R_i^- P_i^- \leq \sum_{j\neq i} \min\{0, \tilde{f}_{ij}\} \leq f_i^* = \alpha_i Q_i^-. \tag{43}$$

Likewise, a strictly positive antidiffusive correction $f_i^* > 0$ is bounded from above by

$$\alpha_i Q_i^+ = f_i^* \le \sum_{j \ne i} \max\{0, \tilde{f}_{ij}\} \le R_i^+ P_i^+ \le m_i Q_i^+. \tag{44}$$

It follows that $0 \le \alpha_i \le m_i$, which proves that $b_i^* \ge 0$ provided that $\tilde{u}_i \ge 0$ and $\tilde{u}_k \ge 0$.

In light of the above, the semi-implicit FCT limiter is positivity-preserving as long as the diagonal coefficients of the matrix B as defined in (20) are nonnegative. The corresponding CFL-like condition (4) for the maximum admissible time step reads

$$(1-\theta)\Delta t \le \min_i |m_i / l_{ii}|. \tag{45}$$

The positivity of the single-step algorithm based on the slack bounds (39)–(40) can be proven in a similar way using the following representation of the right-hand side

$$b_i^* = (m_i - \alpha_i) u_i^n + \alpha_i u_k^n + (1-\theta)\Delta t \sum_j l_{ij} u_j^n. \tag{46}$$

In this case, the limited antidiffusive correction to node i can be estimated as follows

$$(m_i - m_{ii}) Q_i^- \le f_i^* \le (m_i - m_{ii}) Q_i^+ \tag{47}$$

so that $m_i - \alpha_i \ge m_{ii}$. Thus, the right-hand side given by (46) preserves the sign of u^n if the time step satisfies the positivity constraint for all diagonal coefficients

$$(1-\theta)\Delta t \le \min_i |m_{ii} / l_{ii}|. \tag{48}$$

Under the above conditions, the M-matrix property of the preconditioner A is sufficient to guarantee that each solution update is positivity-preserving.

5.4 Convergence behavior

A remark is in order regarding the convergence behavior of the iterative defect correction scheme (18) preconditioned by the low-order operator (19). The converged solution u^{n+1} is supposed to satisfy a nonlinear algebraic system of the form

$$A^* u^{n+1} = B u^n, \qquad A^* u^{n+1} := A u^{n+1} - f^*, \tag{49}$$

where A^* is the nonlinear FCT operator which includes some built-in antidiffusion. Clearly, the rate of convergence will depend on the approximation property of the preconditioner, i.e., on the norm $||A^* - A||$. On the one hand, the operator A as defined in (19) is linear and easy to 'invert' because it is an M-matrix. On the other hand, it represents a rather poor approximation to the original Galerkin operator $M_C - \theta \Delta t K$ which is recovered in the limit $\alpha_{ij} \to 1$. As a result, the convergence of a highly accurate FCT algorithm is likely to slow down as the high-order solution is approached.

In particular, the lumped-mass version, which is obtained by setting $m_{ij} = 0$ in the definition of the raw antidiffusive flux, converges much faster than the one based on the consistent target flux (17). However, mass lumping may have a devastating effect on the

accuracy of a time-dependent solution, as demonstrated by the numerical examples in the next section. At the same time, the high phase accuracy provided by the consistent mass matrix comes at the cost of slower convergence, due to the fact that the preconditioner A is based on M_L rather than M_C. The high-order system (14) which corresponds to $\alpha_{ij} \equiv 1$ is particularly difficult to solve, even though it is linear (see below).

In general, there is a tradeoff between the accuracy of the numerical solution and convergence of the fixed-point iteration (18). Any modification of the flux limiter which makes it possible to accept more antidiffusion has an adverse effect on the convergence rates. Conversely, more diffusive schemes converge better but their accuracy leaves a lot to be desired. The only way to accelerate convergence without sacrificing some accuracy is to use a sophisticated preconditioner which should include limited antidiffusion but remain an M-matrix. In the context of TVD-like methods such nonlinear operators can be assembled from the solution-dependent coefficients involved in the positivity proof [6],[14]. In fact, driving the residual of time-dependent problems to machine zero is hardly worth the effort. Indeed, a half-converged time-accurate solution is probably better than a fully converged one obtained at a much higher cost or using a less accurate discretization.

6 Numerical examples

In order to illustrate the performance of the semi-implicit FCT algorithm, we apply it to a number of time-dependent benchmark problems discretized in space by the standard Galerkin method on a quadrilateral or triangular mesh. The time discretization is performed by the second-order accurate Crank-Nicolson scheme. All numerical solutions were computed by the algorithm (30)–(38) since the single-step version based on (39)–(40) yields virtually identical results in the range of time steps considered below. The goal of this numerical study is to investigate the accuracy of the proposed discretization tools as well as the convergence behavior of the iterative flux/defect correction scheme (18).

6.1 Solid body rotation

Let us start with the two-dimensional benchmark problem proposed by LeVeque [15] which makes it possible to assess the ability of a high-resolution scheme to preserve both smooth and discontinuous profiles. To this end, a slotted cylinder, a sharp cone and a smooth hump are exposed to the nonuniform velocity field $\mathbf{v} = (0.5 - y, x - 0.5)$ and undergo a counterclockwise rotation about the center of the unit square $\Omega = (0,1) \times (0,1)$. Each solid body lies within a circle of radius $r_0 = 0.15$ centered at a point with Cartesian coordinates (x_0, y_0). In the rest of the domain, the solution is initialized by zero. The shapes of the three bodies as depicted in Fig. 2 can be expressed in terms of the normalized distance function for the respective reference point (x_0, y_0) thus:

$$r(x,y) = \frac{1}{r_0}\sqrt{(x-x_0)^2 + (y-y_0)^2}.$$

The center of the slotted cylinder is located at $(x_0, y_0) = (0.5, 0.75)$ and its geometry in

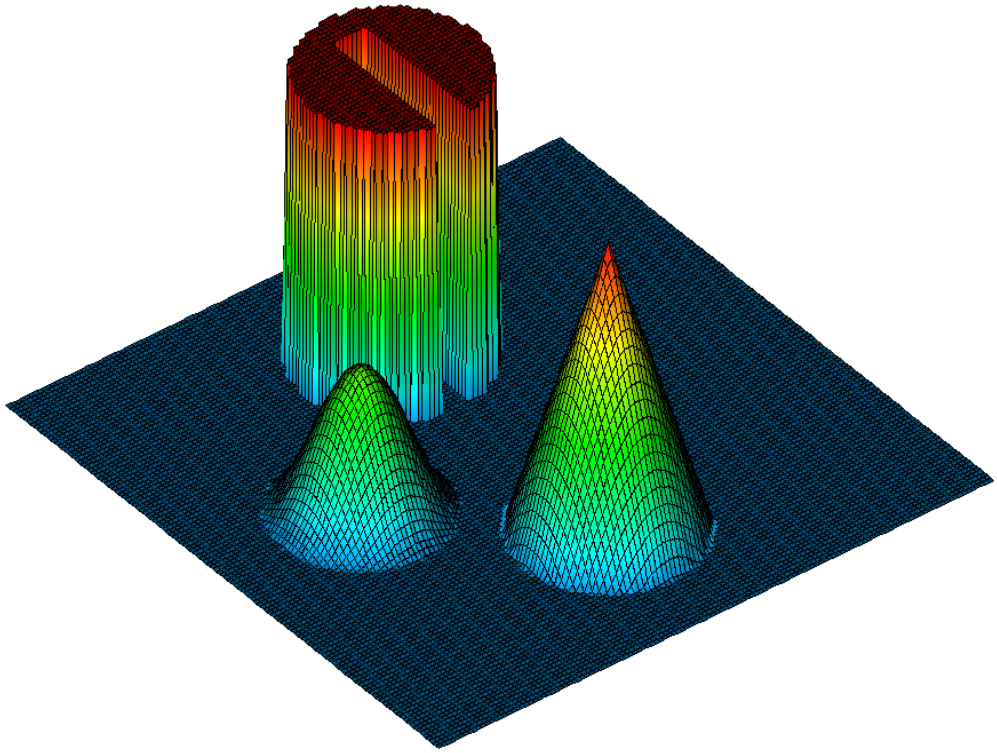

Figure 2: Solid body rotation: initial data / exact solution.

the circular region $r(x,y) \leq 1$ is given by

$$u(x,y,0) = \begin{cases} 1 & \text{if } |x-x_0| \geq 0.025 \ \vee \ y \geq 0.85, \\ 0 & \text{otherwise.} \end{cases}$$

The corresponding analytical expression for the conical body reads

$$u(x,y,0) = 1 - r(x,y), \qquad (x_0,y_0) = (0.5, 0.25),$$

whereas the shape and location of the hump at $t = 0$ are as follows

$$u(x,y,0) = 0.25[1 + \cos(\pi \min\{r(x,y), 1\})], \quad (x_0,y_0) = (0.25, 0.5).$$

After one full revolution ($t = 2\pi$) the exact solution of the continuity equation (6) coincides with the initial data. The numerical solutions presented in Fig. 3 were produced by the semi-implicit FCT algorithm on a uniform mesh of 128×128 bilinear finite elements using the time step $\Delta t = 10^{-3}$. The upper diagram demonstrates the detrimental effect of mass lumping which manifests itself in significant amplitude and phase errors. The lower diagram was computed using the consistent target flux (17) including the contribution of mass antidiffusion. In this case, the shape of the rotating bodies is reproduced very well and even the narrow bridge of the slotted cylinder is largely preserved. This example confirms that time-dependent problems call for the use of a time-accurate high-order scheme based on the consistent mass matrix. A further improvement of phase accuracy is possible in the framework of (semi-implicit) Taylor-Galerkin methods.

FEM-FCT, lumped mass matrix

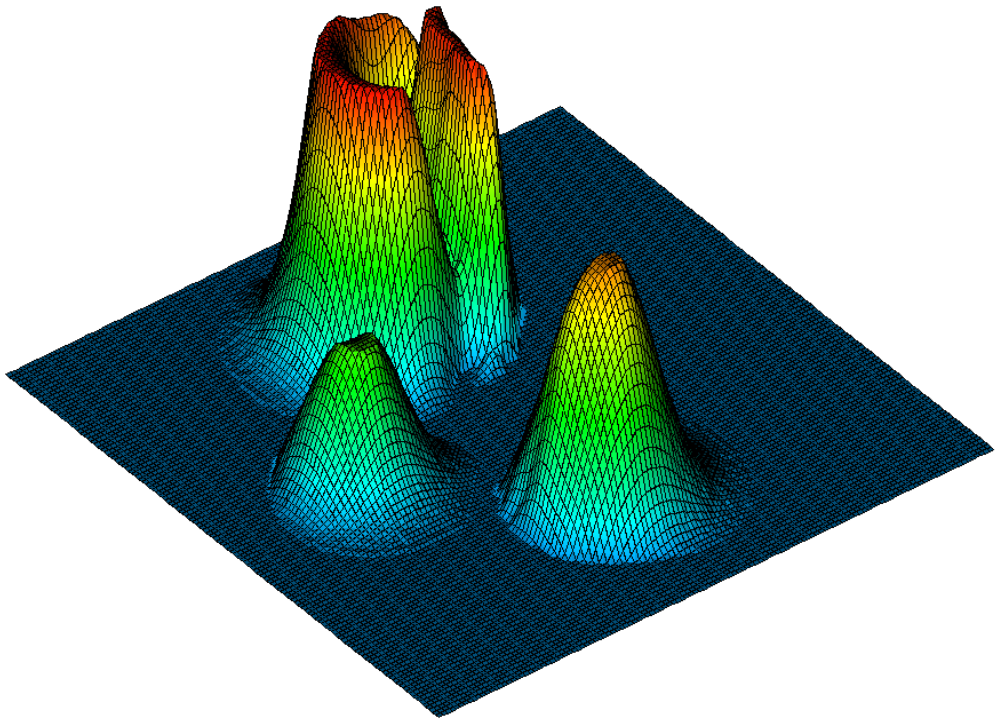

FEM-FCT, consistent mass matrix

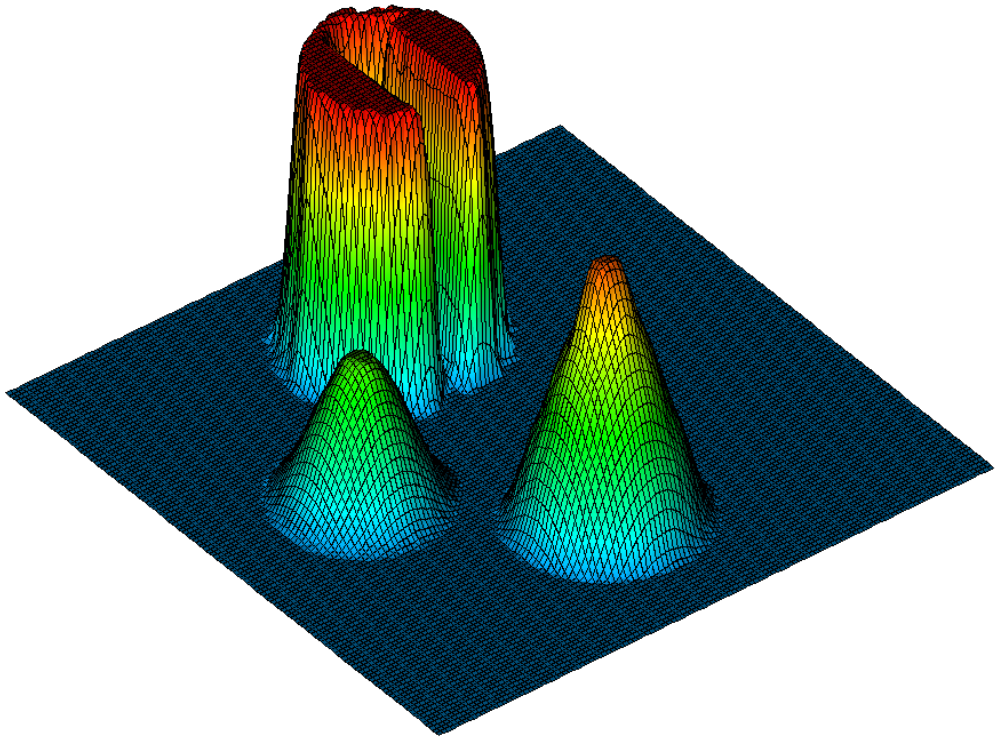

Figure 3: Solid body rotation: numerical solutions at $t = 2\pi$.

6.2 Swirling flow

The second benchmark problem, which was also introduced in [15], deals with a swirling deformation of the initial data by the incompressible velocity field given by

$$v_x = \sin^2(\pi x)\sin(2\pi y), \quad v_y = -\sin^2(\pi y)\sin(2\pi x).$$

The initial condition to be prescribed is a discontinuous function of the spatial coordinates which equals unity within a circular sector of $\pi/2$ radians and zero elsewhere:

$$u(x,y,0) = \begin{cases} 1 & \text{if } (x-1)^2 + (y-1)^2 < 0.64, \\ 0 & \text{otherwise.} \end{cases}$$

In the course of deformation, the mass distribution assumes a complex spiral shape which is nicely resolved by the semi-implicit FCT algorithm. The numerical solution at time $t = 2.5$ calculated using the same mesh and time step as in the previous example is displayed in Fig. 4. The use of a piecewise-linear finite element approximation on a triangular mesh with the same number of nodes yields virtually the same results, see Fig. 5. For the difference between the underlying triangulations to be visible, both solutions were output on coarser meshes consisting of 4,225 vertices. In either case, the evolution details are captured with high precision and the resolution of discontinuities is remarkably crisp. These results compare well to those computed in [12] using flux limiters of TVD type.

6.3 Convection skew to the mesh

In order to compare the convergence behavior of the semi-implicit FEM-FCT algorithm to that of the underlying Galerkin scheme, let us solve equation (6) with $\mathbf{v} = (1,1)$ so that the initial profile is translated along the diagonal of the computational domain $\Omega = (0,1) \times (0,1)$. The numerical study is to be performed for two different initial configurations centered at the reference point $(x_0, y_0) = (0.3, 0.3)$

TP1 The first test problem corresponds to the discontinuous initial condition

$$u(x,y,0) = \begin{cases} 1 & \text{if } \max\{|x-x_0|, |y-y_0|\} \le 0.1, \\ 0 & \text{otherwise.} \end{cases} \tag{50}$$

TP2 The second test problem deals with translation of a smooth function defined as

$$u(x,y,0) = \frac{1}{4}[1+\cos(10\pi(x-x_0))][1+\cos(10\pi(y-y_0))] \tag{51}$$

within the circle $\sqrt{(x-x_0)^2 + (y-y_0)^2} \le 0.1$ and equal to zero elsewhere.

Figure 6 displays the approximate solutions at $t = 0.5$ computed using $\Delta t = 10^{-3}$ on a quadrilateral mesh consisting of 128×128 bilinear elements. The left diagrams were produced by the consistent-mass FCT algorithm which yields nonoscillatory solutions bounded by 0 and 1. The underlying high-order scheme remains stable but gives rise to nonphysical undershoots and overshoots, as seen in the right diagrams.

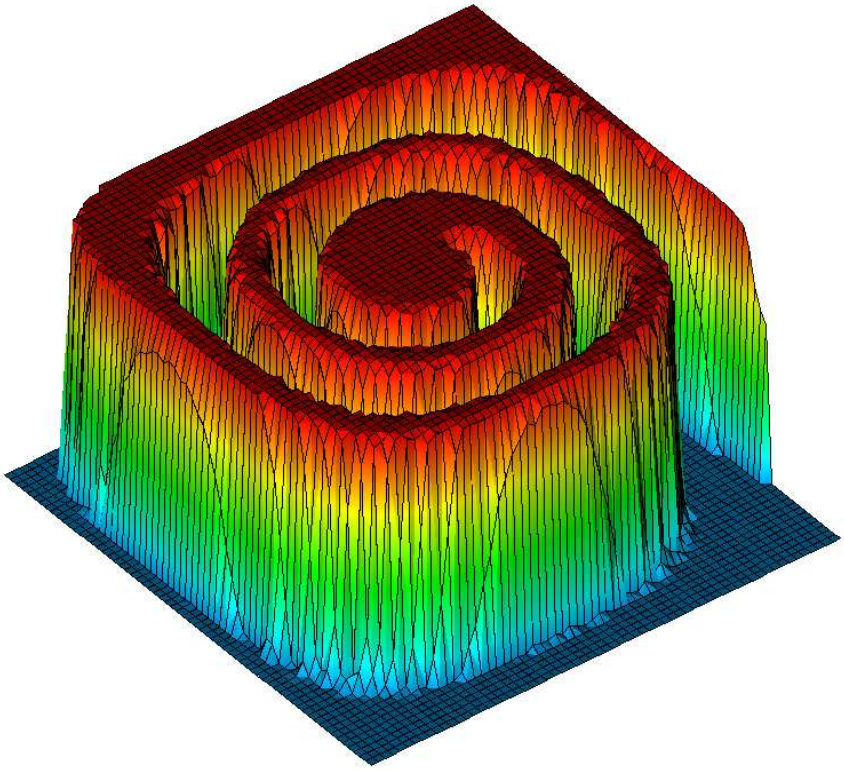

Figure 4: Swirling deformation on a quadrilateral mesh, $t = 2.5$.

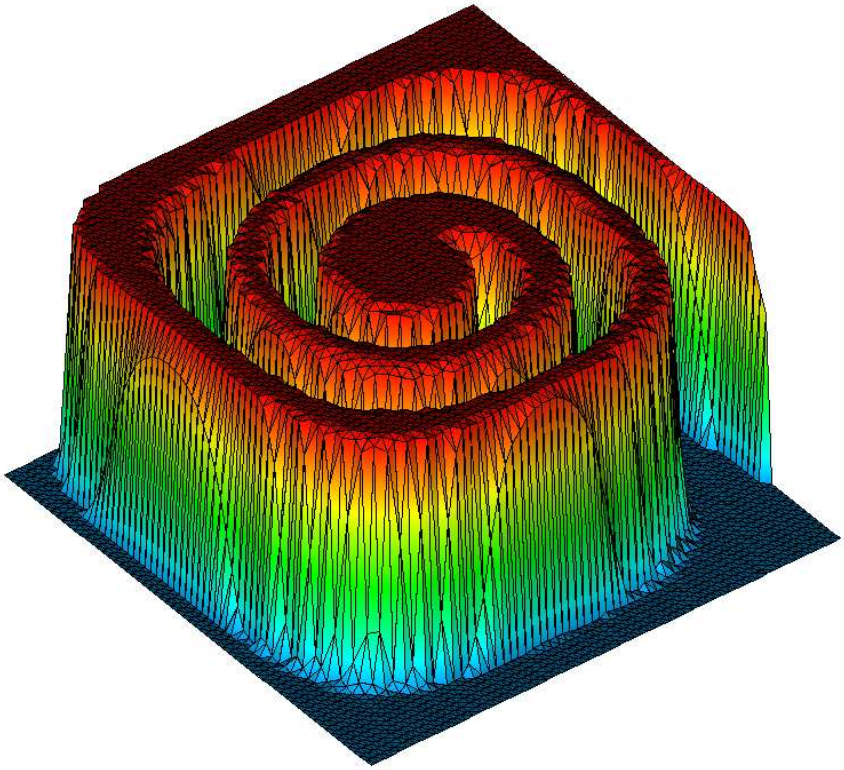

Figure 5: Swirling deformation on a triangular mesh, $t = 2.5$.

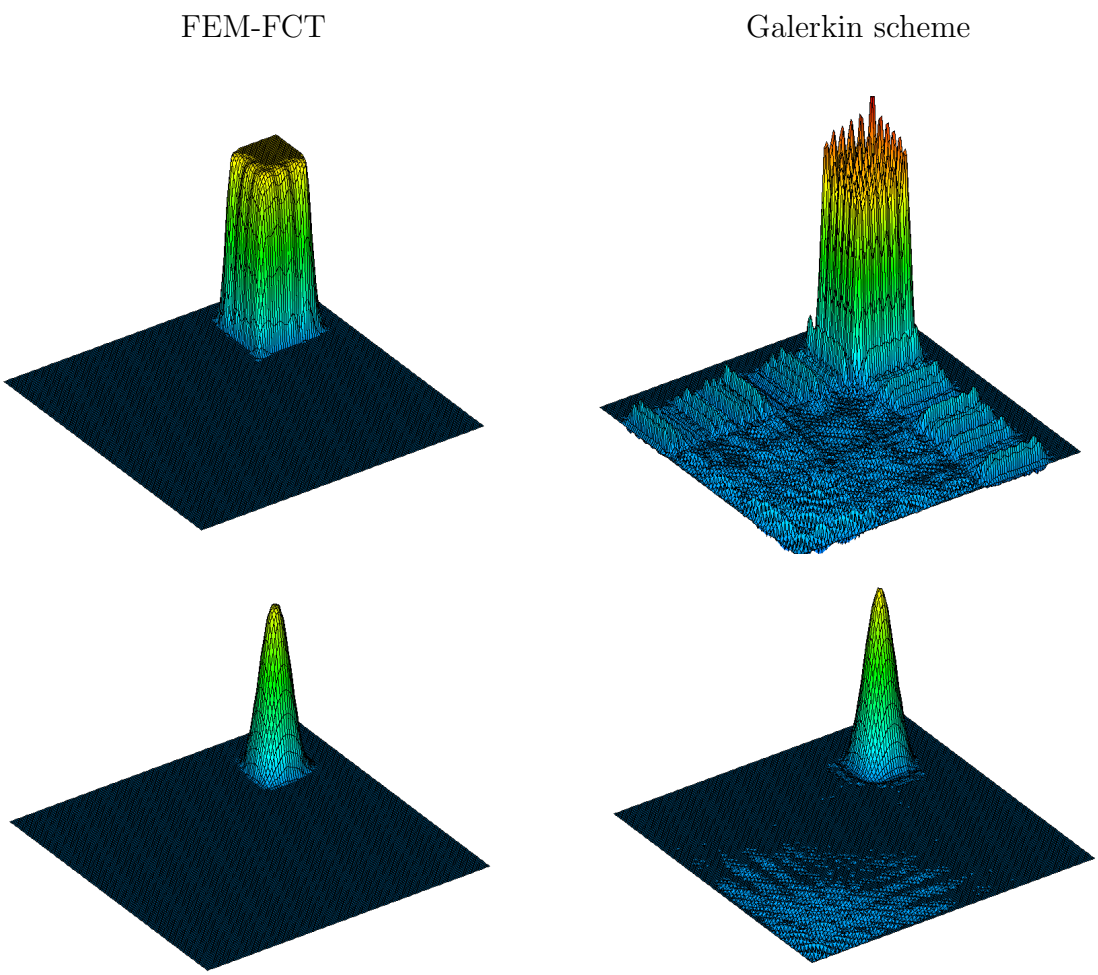

Figure 6: Convection skew to the mesh: 128×128 Q_1-elements, $t = 0.5$.

In either case, the numerical solution was computed in an iterative way using the defect correction scheme (18) preconditioned by the low-order operator (19). The stopping criterion was based on the Euclidean norm of the residual vector

$$r = Au^{n+1} - Bu^n - f^*, \qquad ||r|| = \sqrt{r^T r} \tag{52}$$

which was required to satisfy the inequality $||r|| \leq 10^{-4}$. The difference between the exact solution u and its finite element approximation u_h was measured in the L_1-norm

$$||u - u_h||_1 = \int_\Omega |u - u_h| \, \mathrm{d}x \approx \sum_i m_i |u(x_i, y_i) - u_i| \tag{53}$$

as well as in the L_2-norm defined by the following formula

$$||u - u_h||_2^2 = \int_\Omega |u - u_h|^2 \, \mathrm{d}x \approx \sum_i m_i |u(x_i, y_i) - u_i|^2, \tag{54}$$

where $m_i = \int_\Omega \varphi_i \, \mathrm{d}x$ are the diagonal coefficients of the lumped mass matrix. Furthermore, the global minimum $u_{\min} = \min_i u_i$ and maximum $u_{\max} = \max_i u_i$ of the discrete solution u_h were compared to their analytical values 0 and 1.

Tables 1 and 2 illustrate the convergence behavior of the iterative flux/defect correction scheme as applied to the test problems TP1 and TP2 on three successively refined meshes. The first three columns in each table display the refinement level NLEV, the number of vertices/nodes NVT and the total number of outer iterations NDC required to compute the numerical solution at $t = 0.5$. The different performance of the four algorithms under consideration supports the arguments presented in Section 5.4. In particular, it can readily be seen that the use of the consistent mass matrix results in a much better accuracy but the convergence slows down, whereas the lumped-mass version is less accurate but much more efficient. In the difference $||u^{n+1} - u^n||$ is large, mass antidiffusion affects the convergence rates even stronger than the convective part of the antidiffusive flux. Since the latter is proportional to Δt, the mass lumping error plays a dominant role at small time steps such that $A \approx M_L$. Note that the consistent-mass Galerkin scheme faces severe convergence problems and the error may even increase as the mesh is refined (see Table 2).

On the other hand, the results computed by the semi-implicit FCT algorithm exhibit a monotone grid convergence as well as some improvement of the convergence rates. Even the consistent-mass version converges slowly but surely to a nonoscillatory time-accurate solution. For large time steps, the single-step implementation based on (39)–(40) would be more diffusive and converge faster. However, for time steps as small as the one employed

FEM-FCT algorithm / consistent mass matrix

NLEV	NVT	NDC	$\|\|u-u_h\|\|_1$	$\|\|u-u_h\|\|_2$	$u_{\min}$	$u_{\max}$
6	4,225	2,500	1.1737e-2	6.2176e-2	0.0	1.0
7	16,641	2,461	7.3688e-3	4.8577e-2	0.0	1.0
8	66,049	2,489	4.7039e-3	3.8715e-2	0.0	1.0

FEM-FCT algorithm / lumped mass matrix

NLEV	NVT	NDC	$\|\|u-u_h\|\|_1$	$\|\|u-u_h\|\|_2$	$u_{\min}$	$u_{\max}$
6	4,225	751	1.9356e-2	8.4294e-2	0.0	0.9988
7	16,641	1,000	1.2402e-2	6.5356e-2	0.0	1.0000
8	66,049	1,014	7.8511e-3	5.1182e-2	0.0	1.0000

Galerkin scheme/ consistent mass matrix

NLEV	NVT	NDC	$\|\|u-u_h\|\|_1$	$\|\|u-u_h\|\|_2$	$u_{\min}$	$u_{\max}$
6	4,225	4,666	3.6283e-2	7.4952e-2	-0.2557	1.4505
7	16,641	7,379	2.7340e-2	5.8124e-2	-0.2743	1.3797
8	66,049	13,852	2.3000e-2	5.2536e-2	-0.4437	1.4080

Galerkin scheme / lumped mass matrix

NLEV	NVT	NDC	$\|\|u-u_h\|\|_1$	$\|\|u-u_h\|\|_2$	$u_{\min}$	$u_{\max}$
6	4,225	1,000	6.5181e-2	1.3073e-1	-0.4022	1.5608
7	16,641	1,423	4.7055e-2	9.8663e-2	-0.4340	1.5732
8	66,049	1,500	3.5126e-2	8.0298e-2	-0.3713	1.5628

Table 1: Convection skew to the mesh: discontinuous initial data.

FEM-FCT algorithm / consistent mass matrix

NLEV	NVT	NDC	$\|\|u-u_h\|\|_1$	$\|\|u-u_h\|\|_2$	$u_{\min}$	$u_{\max}$
6	4,225	2,486	1.4799e-3	9.2813e-3	0.0	0.8562
7	16,641	1,833	4.3436e-4	2.7820e-3	0.0	0.9418
8	66,049	2,867	1.7887e-4	1.2032e-3	0.0	0.9740

FEM-FCT algorithm / lumped mass matrix

NLEV	NVT	NDC	$\|\|u-u_h\|\|_1$	$\|\|u-u_h\|\|_2$	$u_{\min}$	$u_{\max}$
6	4,225	1,000	4.2704e-3	2.7827e-2	0.0	0.7308
7	16,641	1,000	1.7834e-3	1.1294e-2	0.0	0.9218
8	66,049	736	7.6982e-4	4.6142e-3	0.0	0.9612

Galerkin scheme / consistent mass matrix

NLEV	NVT	NDC	$\|\|u-u_h\|\|_1$	$\|\|u-u_h\|\|_2$	$u_{\min}$	$u_{\max}$
6	4,225	2,500	1.3961e-3	2.6234e-3	-0.0158	0.9890
7	16,641	6,437	1.8892e-3	3.9001e-3	-0.0480	0.9925
8	66,049	13,700	2.3237e-3	8.1553e-3	-0.1363	1.0012

Galerkin scheme / lumped mass matrix

NLEV	NVT	NDC	$\|\|u-u_h\|\|_1$	$\|\|u-u_h\|\|_2$	$u_{\min}$	$u_{\max}$
6	4,225	1,000	1.0904e-2	4.2409e-2	-0.1911	0.8809
7	16,641	1,000	3.4837e-3	1.4234e-2	-0.0811	1.0098
8	66,049	1,000	1.3092e-3	4.3179e-3	-0.0322	1.0046

Table 2: Convection skew to the mesh: smooth initial data.

in this section, it would be just as accurate and converge at the same rate as the algorithm (30)–(38). The values of $u_{\max}$ in Table 2 reveal that flux correction may lead to undesirable 'peak clipping', which is a well-known phenomenon discussed, e.g., in [12],[23]. On the other hand, the associated high-order solution is corrupted by undershoots and overshoots which are particularly large for discontinuous initial data (Table 1) and less pronounced for the smooth cosine hill (Table 2). These nonphysical oscillations result in a dramatic loss of accuracy and slow/no convergence, so that the results are inferior to those produced by the FEM-FCT algorithm using the same parameter settings. Since the latter converges faster than the Galerkin scheme, it is more efficient than semi-explicit flux correction (24)–(29) which represents a positivity-preserving postprocessing of the high-order predictor.

Of course, the linear system (14) could be solved in one step without resorting to defect correction. However, this straightforward approach would lead to a severe deterioration of linear convergence rates. Indeed, the high-order operator $M_C - \theta\Delta tK$ is much harder to 'invert' than the preconditioner A which enjoys the M-matrix property. In many cases, the high-order solution may prove prohibitively expensive or even impossible to compute in such a brute-force way, unless a direct solver is employed. Hence, even linear high-order systems of the form (15) call for the use of iterative defect correction [8].

7 Conclusions

The semi-implicit approach to flux correction of FCT type leads to a robust and efficient special-purpose algorithm for time-dependent problems discretized in space by the finite element method. The accuracy of the resulting scheme improves as the time step is refined and the consistent mass matrix can be included in a positivity-preserving fashion. The new limiting strategy makes it possible to avoid a repeated computation of the nodal correction factors at each outer iteration. Therefore, the use of an implicit time-stepping method pays off inspite of the CFL-like condition to be satisfied by the time step in the case $\theta < 1$. For sufficiently small time steps, the new algorithm is more accurate and/or efficient than the algebraic flux correction schemes proposed in [8],[10]. On the other hand, it is not to be recommended for steady-state computations which call for the use of large time steps. In this case, it is worthwhile to redefine the underlying constraints as explained in [14] and switch to an upwind-biased limiting strategy. A promising direction for further research is the design of characteristic FCT limiters for the Euler equations [25] on the basis of (39)–(40). Indeed, the use of upper/lower bounds depending on the local extrema of u^n rather than $\tilde{u}$ makes it possible to decouple the discrete Jacobian operators and limit them separately as in the case of characteristic TVD methods [13].

References

[1] J. P. Boris and D. L. Book, Flux-corrected transport. I. SHASTA, A fluid transport algorithm that works. *J. Comput. Phys.* **11** (1973) 38–69.

[2] D. L. Book, The conception, gestation, birth, and infancy of FCT. In: D. Kuzmin, R. Löhner and S. Turek (eds.) *Flux-Corrected Transport: Principles, Algorithms, and Applications*. Springer, 2005, 5-28.

[3] J. Donea, L. Quartapelle and V. Selmin, An analysis of time discretization in the finite element solution of hyperbolic problems. *J. Comput. Phys.* **70** (1987) 463–499.

[4] A. Jameson, Computational algorithms for aerodynamic analysis and design. *Appl. Numer. Math.* **13** (1993) 383-422.

[5] A. Jameson, Positive schemes and shock modelling for compressible flows. *Int. J. Numer. Meth. Fluids* **20** (1995) 743–776.

[6] T. Jongen and Y.P. Marx, Design of an unconditionally stable, positive scheme for the $K-\varepsilon$ and two-layer turbulence models. *Comput. Fluids* **26** (1997) no. 5, 469-487.

[7] D. Kuzmin, Positive finite element schemes based on the flux-corrected transport procedure. In: K. J. Bathe (ed.), *Computational Fluid and Solid Mechanics*, Elsevier, 887-888 (2001).

[8] D. Kuzmin and S. Turek, Flux correction tools for finite elements. *J. Comput. Phys.* **175** (2002) 525-558.

[9] D. Kuzmin, M. Möller and S. Turek, Multidimensional FEM-FCT schemes for arbitrary time-stepping. *Int. J. Numer. Meth. Fluids* **42** (2003) 265-295.

[10] D. Kuzmin, M. Möller and S. Turek, High-resolution FEM-FCT schemes for multidimensional conservation laws. *Computer Meth. Appl. Mech. Engrg.* **193** (2004) 4915-4946.

[11] D. Kuzmin and S. Turek, High-resolution FEM-TVD schemes based on a fully multidimensional flux limiter. *J. Comput. Phys.* **198** (2004) 131-158.

[12] D. Kuzmin and M. Möller, Algebraic flux correction I. Scalar conservation laws. In: D. Kuzmin, R. Löhner and S. Turek (eds.) *Flux-Corrected Transport: Principles, Algorithms, and Applications*. Springer, 2005, 155-206.

[13] D. Kuzmin and M. Möller, Algebraic flux correction II. Compressible Euler equations. In: D. Kuzmin, R. Löhner and S. Turek (eds.) *Flux-Corrected Transport: Principles, Algorithms, and Applications*. Springer, 2005, 207-250.

[14] D. Kuzmin, On the design of general-purpose flux limiters for implicit FEM with a consistent mass matrix. Technical report **283**, University of Dortmund, 2005

[15] R. J. LeVeque, High-resolution conservative algorithms for advection in incompressible flow. *Siam J. Numer. Anal.* **33** (1996) 627–665.

[16] R. Löhner, K. Morgan, J. Peraire and M. Vahdati, Finite element flux-corrected transport (FEM-FCT) for the Euler and Navier-Stokes equations. *Int. J. Numer. Meth. Fluids* **7** (1987) 1093–1109.

[17] R. Löhner, K. Morgan, M. Vahdati, J. P. Boris and D. L. Book, FEM-FCT: combining unstructured grids with high resolution. *Commun. Appl. Numer. Methods* **4** (1988) 717–729.

[18] R. Löhner and J. D. Baum, *30 Years of FCT: Status and Directions*. In: D. Kuzmin, R. Löhner and S. Turek (eds.) *Flux-Corrected Transport: Principles, Algorithms, and Applications*. Springer, 2005, 251-296.

[19] S. Turek, *Efficient Solvers for Incompressible Flow Problems: An Algorithmic and Computational Approach*, LNCSE **6**, Springer, 1999.

[20] S. Turek and D. Kuzmin, Algebraic flux correction III. Incompressible flow problems. In: D. Kuzmin, R. Löhner and S. Turek (eds.) *Flux-Corrected Transport: Principles, Algorithms, and Applications*. Springer, 2005, 251-296.

[21] R. W. C. P. Verstappen and A. E. P. Veldman, Preserving symmetry in convection-diffusion schemes. In: D. Drikakis and J. Geurts (eds.) *Turbulent flow computation*, Fluid Mechanics and its Applications **6**. Dordrecht: Kluwer, 2002.

[22] R. W. C. P. Verstappen and A. E. P. Veldman, Symmetry-preserving discretization of turbulent flow. *J. Comput. Phys.* **187** (2003) 343-368.

[23] S. T. Zalesak, Fully multidimensional flux-corrected transport algorithms for fluids. *J. Comput. Phys.* **31** (1979) 335–362.

[24] S. T. Zalesak, A preliminary comparison of modern shock-capturing schemes: linear advection. In: R. Vichnevetsky and R. Stepleman (eds.) *Advances in Computer Methods for PDEs*. Publ. IMACS, 1987, 15-22.

[25] S. T. Zalesak, The design of Flux-Corrected Transport (FCT) algorithms for structured grids. In: D. Kuzmin, R. Löhner and S. Turek (eds.) *Flux-Corrected Transport: Principles, Algorithms, and Applications*. Springer, 2005, 29-78.